Computational and Structural Biotechnology Journal 18 (2020) 3877–3889

COMPUTATIONAL AND STRUCTURAL BIOTECHNOLOGY JOURNAL

journal homepage: www.elsevier.com/locate/csbj

A mathematical model for understanding synergistic regulations and paradoxical feedbacks in the shoot apical meristem

Ziyi Liu [a], Elena D. Shpak [b], Tian Hong [b,c,*]

[a] Graduate School of Genome Science and Technology, The University of Tennessee, Knoxville, TN, United States
[b] Department of Biochemistry & Cellular and Molecular Biology, The University of Tennessee, Knoxville, TN, United States
[c] National Institute for Mathematical and Biological Synthesis, Knoxville, TN, United States

ARTICLE INFO

Article history:
Received 20 August 2020
Received in revised form 9 November 2020
Accepted 10 November 2020
Available online 21 November 2020

Keywords:
EPFL
Shoot apical meristem
Stem cell niche
Paradoxical feedback

ABSTRACT

The shoot apical meristem (SAM) is the primary stem cell niche in plant shoots. Stem cells in the SAM are controlled by an intricate regulatory network, including negative feedback between WUSCHEL (WUS) and CLAVATA3 (CLV3). Recently, we identified a group of signals, Epidermal Patterning Factor-Like (EPFL) proteins, that are produced at the peripheral region and are important for SAM homeostasis. Here, we present a mathematical model for the SAM regulatory network. The model revealed that the SAM uses EPFL and signals such as HAIRY MERISTEM from the middle in a synergistic manner to constrain both *WUS* and *CLV3*. We found that interconnected negative and positive feedbacks between WUS and CLV3 ensure stable *WUS* expression in the SAM when facing perturbations, and the positive feedback loop also maintains distinct cell populations containing WUS^{on} and $CLV3^{on}$ cells in the apical-basal direction. Furthermore, systematic perturbations of the parameters revealed a tradeoff between optimizations of multiple patterning features. Our results provide a holistic view of the regulation of SAM patterning in multiple dimensions. They give insights into how *Arabidopsis* integrates signals from lateral and apical-basal axes to control the SAM patterning, and they shed light into design principles that may be widely useful for understanding regulatory networks of stem cell niche.

1. Introduction

Spatiotemporal regulation of cell populations in stem cell niches is critical for plants and animals during developmental and homeostatic conditions [1–5]. The shoot apical meristem (SAM) of *Arabidopsis thaliana* is one of the most extensively studied model systems for understanding stem cell niches in plants. The dome-shaped SAM harbors stem cells that are located in the epidermal and subepidermal layers. Under normal conditions these cells are characterized by the high expression of *CLAVATA3* (*CLV3*), which encodes a secreted peptide that can diffuse to neighboring cells and regulate their gene expression [6]. The patterning and size of the SAM remain stable in mature plants, suggesting tight regulation of stem cell populations. Previous studies have revealed crucial mechanisms for regulating these cells in the apical-basal axis of the SAM. Particularly, the number of stem cells is maintained by *WUSCHEL* (*WUS*), which is expressed in cells of the organizing center below the subepidermal layers of the SAM [7,8]. WUS protein moves to the upper layers and activates *CLV3* expression, whereas the diffusible CLV3 peptide suppresses the expression of *WUS* [9–11]. This negative feedback loop is considered the core circuit controlling the size of the SAM and the number of stem cells in this region [9,10,12]. More recent discoveries show that the separation of *WUS* and *CLV3* expressing regions is driven by additional signals originating from the basal zones of the SAM, such as high concentrations of WUS and/or HAIRY MERISTEM (HAM) [13–15], and these signals prevent *CLV3* expression below the subepidermal layer. Mathematical models have been used in numerous studies to describe the dynamics of gene activities in the SAM quantitatively, and have improved our understanding of the complex molecular and cellular networks controlling SAM patterning [11,13,16–25]. These models have revealed the key role of negative feedback in maintaining homeostasis, as well as the mechanisms underlying the separation between *CLV3* and *WUS* expressing domains. While these experimental and computational studies provided ample information about regulatory networks along the apical-basal axis, regulatory mechanisms in the lateral direction of the SAM remain unclear.

* Corresponding author at: Department of Biochemistry & Cellular and Molecular Biology, The University of Tennessee, Knoxville, TN, United States.
E-mail address: hongtian@utk.edu (T. Hong).

https://doi.org/10.1016/j.csbj.2020.11.017

For example, it was proposed that some 'pocket-like' signals restrict *CLV3* expression in both the apical-basal and lateral directions [22], but currently there is no experimental evidence showing the existence of any inhibitory factor with such an expression pattern. Although WUS has been shown to play a role in restricting the *CLV3* expression laterally [13,15,26,27], theoretical reconstruction of correct SAM patterning still requires some additional hypothetical 'positional cues' that constrain *CLV3* expression [27]. Therefore, our understanding of mechanisms underlying lateral boundary of the *CLV3* and/or *WUS* expressing domains in the SAM is incomplete.

Recently, we have identified a group of potent signals, Epidermal Patterning Factor-Like (EPFL) proteins, that originate from the peripheral zone of SAM and inhibit *CLV3* and *WUS* expression [28,29]. EPFL signals are communicated by four diffusive ligands: EPFL1, EPFL2, EPFL4, and EPFL6 [28]. The loss of these ligands caused the upregulation of both *WUS* and *CLV3* and increased the size of the SAM, suggesting that these signals play an essential role in maintaining the stem cell population in the SAM, and their perturbation can override the negative feedback loop [29]. However, it is unclear how the SAM integrates information from the apical-basal direction with that from the lateral direction, and how multiple signals synergistically control SAM patterning.

To obtain insights into these questions, we built a mathematical model describing the intracellular and intercellular regulatory networks in the meristem. We perturbed the model to examine the key regulatory elements (e.g. EPFL and HAM) controlling the gene expression patterns in the middle and peripheral regions of the SAM, and to unravel the roles of interconnected negative and positive feedbacks between WUS and CLV3 in SAM patterning. We further used three new metrics of patterning to explore functional objectives that may constraint the kinetic rate constants underlying regulations of key genes: 1) downregulation of *WUS* expression in the lateral region of the SAM; 2) stability of total WUS concentration in the SAM in the presence of perturbations; and 3) diverse cell populations that highly express either *WUS* or *CLV3* in the middle of the SAM. These analyses provide a holistic view of the principles governing the SAM patterning.

2. Results

2.1. A mathematical model recapitulates known phenotypes of SAM patterning under normal and perturbed conditions

Previous mathematical models of SAM patterning have been focused on the negative feedback between WUS and CLV3, as well as other factors controlling their expressions along the apical-basal axis [11,13,16–20,22–25]. Here, we built a two-dimensional model incorporating elements of these previous models with the potent lateral regulator EPFL that was recently characterized (Fig. 1A) [28,29]. We considered 51 cells (a minimum number of cells that reflects multilayer patterning of the SAM in terms of key factors [13]) organized in a dome-shaped structure. This structure contains six layers of cells (L1-L6) for which gene expression patterning is critical for development [13,14]. In each cell, concentrations of six interacting molecules were described with ordinary differential equations (ODEs) based on the gene regulatory network shown in Fig. 1A (see Methods for details). Key assumptions about the regions producing the regulatory molecules are illustrated in Fig. 1B (See Methods and Table 1 for details). Our assumptions also include diffusion/movement of EPFL, WUS and CLV3 in all directions. We sought to obtain a comprehensive view of gene regulation in SAM patterning by simulating and analyzing this model under various conditions.

We first fit our model to SAM patterning under normal conditions (wild type, WT) as well as several phenotypes in terms of distributions of key molecules due to genetic perturbations of several regulators. We identified a representative parameter set that allows the model to reproduce experimentally observed phenotypes (Fig. 1C–I, Table 2).

In the simulated wild type, *WUS* and *CLV3* were expressed in confined regions near the central axis of the SAM, while their proteins diffused (CLV3) or moved (WUS) broadly to other regions (Fig. 1C). Along the apical-basal axis, a moderate amount of WUS moved to L1 layer, where it maintained the expression of *CLV3*. Similarly, a moderate amount of CLV3 diffused to the meristem rib (Fig. 1C). Notably, both *WUS* and *CLV3* expressing regions are limited by lateral boundaries, whereas their expressions in the apical-basal direction are anticorrelated with each other, with the L1 layer expressing *CLV3* but not *WUS*, and bottom layers only expressing *WUS* (Fig. 1C). EPFL was distributed differentially within and across layers, due to the assumption of its isotropic diffusion, and this established a lateral-middle spatial gradient (Fig. 1C). In the *wus* mutant, no *CLV3* expression was observed as we expected from the gene regulatory network (Fig. 1A and D) [30,31]. The lateral confinement of both *WUS* and *CLV3* was lost upon the removal of signaling triggers by EPFL (Fig. 1E): *WUS* expression had a moderate lateral expansion, whereas *CLV3* had a dramatic expansion in the epidermal (L1) layer and the L2 layer (note that the *erf* mutant in this study refers to the absence of multiple ERf receptors, which requires knocking out three genes experimentally). These observations are consistent with recent experimental findings [30,32]. Interestingly, the model showed that the anticorrelation pattern of *WUS* and *CLV3* expressions was largely maintained in this mutant despite their own expansions (Fig. 1E). The model reproduced the well-known phenotype of the *CLV3* knockout (KO): the *WUS* expressing region expanded both apically and laterally upon the loss of *CLV3* (Fig. 1F). Moreover, the expression in the meristem rib was increased from the level in the wildtype (Fig. 1C and F), indicating the inhibitory effect of CLV3 diffused to this region. The model showed that in the absence of both EPFL and CLV3 signals, *WUS* had a dramatic increase in expression across the SAM (Fig. 1G). The model also showed that the anticorrelated *WUS-CLV3* expression pattern was lost in the absence of HAM (Fig. 1H), and this co-expression of *WUS* and *CLV3* in the organizing center with HAM KO was observed previously [13,33]. Interestingly, there was a moderate decrease of *CLV3* expression in the central zone with the loss of HAM compared to the wild type (Fig. 1H), even though the central zone *CLV3* expression was not regulated by HAM directly in our model (see Methods). The decrease of *CLV3* expression in the central zone was because of the negative feedback between WUS and CLV3: the moderately decreased *WUS* expression upon the expansion of *CLV3* expression to the meristem rib reduced the availability of WUS protein in the central zone. This reduction in turn decreased the *CLV3* expression in the central zone, but not in the meristem rib due to the dominant effect of the loss of HAM. The alteration of the *CLV3* expression pattern in the *ham* mutant is consistent with a recent report (Zhou et al., 2018). Nonetheless, a significant level of *WUS* expression was maintained in the meristem rib (Schulze et al., 2010), and this level of WUS in the SAM was critical for the overall gene patterns in the region, as manifested in the phenotype upon the complete loss of WUS (Fig. 1D). In addition to these genetic perturbations, our model recapitulated the observed stability of the WUS expression when the *CLV3* expression was increased by 10-fold [34] (Fig. S1A). We summarized the key SAM expression patterns that are captured by the model and their supporting experimental evidence in Table 2. In conclusion, our model captures the effects of perturbations of key genes that regulate SAM patterning in both apical-basal and lateral directions.

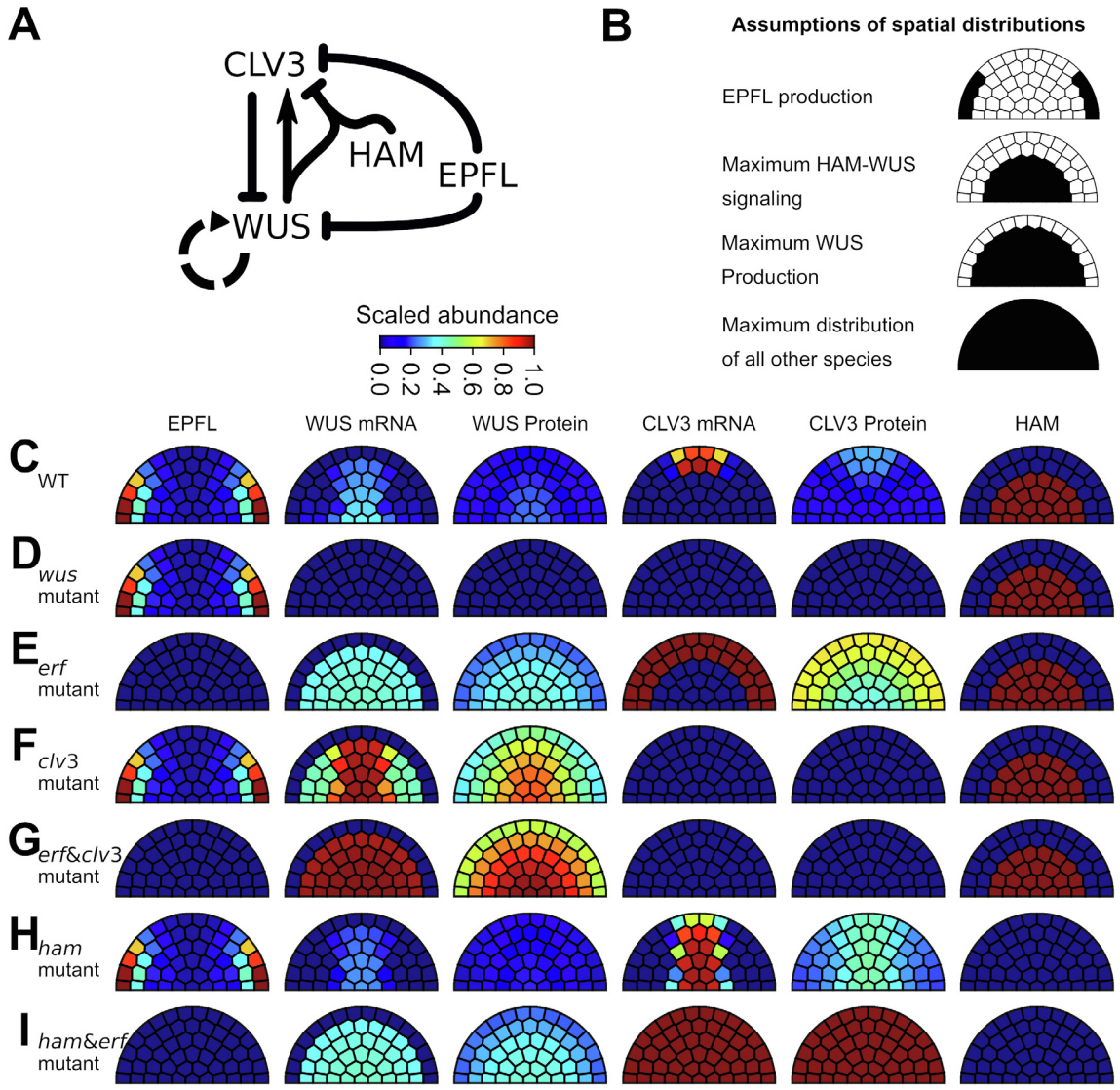

Fig. 1. A mathematical model of SAM captures roles of key regulators of SAM patterning. A. Influence diagram for key molecules regulating SAM patterning. ARR and cytokinin were implicitly modeled (WUS activates itself in the model). A single variable was used to describe the combined signaling of WUS and HAM. Arrows indicate experimentally supported regulations (Table 1). B. Key assumptions about spatial distribution of SAM regulators. Black regions highlight cells that were assumed to have the capacity to produce the denoted molecules. Maximum signaling/distribution/production refers to the distributions of denoted production or signaling in the absence of inhibitors and in the presence of activators. EPFL, CLV3 and WUS proteins were allowed to move between neighboring cells. C-J. Steady state distributions of SAM regulators under various conditions. All mutants were simulated by removing the production of the denoted molecules. All simulations were performed under initial conditions with low amount (=0) of all molecules across SAM.

The model makes an immediate prediction that the loss of HAM and EPFL will cause dramatic expansion of the CLV3-expressing region, as well as expansion of the *WUS*-expressing region in both the lateral and apical-basal axes (Fig. 1I). In the following sections, we describe specific insights and other predictions that we obtained from the model.

2.2. Differential roles of EPFLs and CLV3 in regulating SAM patterning

It has been previously shown that *WUS* expression in the middle SAM is essential for maintaining stem cell populations [7,8,26]. In contrast, *WUS* expression in the lateral region of the SAM is associated with abnormal development [10,30]. These observations suggest that the two regions may require different modes of regulation. To gain deeper understanding of the roles of EPFL and CLV3 in limiting the *WUS* expression region, we focused on two SAM areas described in the model (Fig. 2A). Region 1 (Fig. 2A, blue) includes cells near the middle apical-basal axis of the SAM, whereas Region 2 (Fig. 2A, Indian red) includes cells in the peripheral zone. In terms of our simulation results (Fig. 1C), Region 1 was defined as cells that express either *WUS* or *CLV3* under the wild-type condition, whereas Region 2 was defined as cells that neither express *WUS* nor *CLV3* under the same condition.

We quantified the amount of *WUS* mRNA (in an arbitrary unit, or a.u.) in these two areas based on our simulations. We found that upon the loss of EPFLs there was a moderate increase of total *WUS* expression near the middle apical-basal axis, but the increase was more prominent in the *clv3* mutant (Fig. 2B, blue). This increase in the *clv3* mutant is comparable to that observed in the *erf-clv3* mutant, suggesting that the apical-basal boundary of the *WUS*-expressing zone is primarily controlled by CLV3. In contrast to the dominant role of CLV3 in Region 1, EPFL and CLV3 both control *WUS* expression in Region 2: the loss of either factor (single-mutants) resulted in a significant increase of *WUS* expression,

Table 1
Key assumptions of the model.

Assumption	Reference for experimental evidence
Ligands EPFL are produced in the lateral region of the SAM, but are diffused broadly in the SAM	[28]
EPFL inhibits *CLV3* and *WUS* expression	[29]
CLV3 inhibits *WUS* expression, and WUS activates *CLV3* expression	[9–11]
WUS activates its own expression (for example: an ARR-Cytokinin-*WUS* loop)	[23,39,58,59]
HAM inhibits *CLV3* expression	[13]
HAM and WUS synergize to exert transcriptional regulation	[13,49]
HAM is expressed in the lower middle region of the SAM	[13]
WUS may be expressed broadly in the SAM, except for L1 layer	[9,10]
CLV3 may be expressed broadly in the SAM	[13,56,63]
WUS and CLV3 move/diffuse to neighboring cells in the SAM	[11,55,56]

* The phrase 'may be expressed' is used when the model allows the expression, but it is inhibited by relevant inhibitors when they are present.

Table 2
Known SAM gene expression patterns captured by the model.

Genetic background	Description of patterning	Reference for experimental evidence
Wild type	*CLV3* is expressed in the top middle region of the SAM	[6,10,31,56,57]
Wild type	*WUS* is expressed in the lower middle region of the SAM	[6,8–10,57]
wus mutant	No *CLV3* expression	[30,31]
clv3 mutant	Increased *WUS* expression in the SAM as compared to wild type, including lateral region	[9,63]
erf mutant	Increased *WUS* expression in the SAM as compared to wild type, including lateral region	[32]
erf mutant	Increased and broader *CLV3* expression as compared to wild type	[30,32]
clv3-erf mutant	Highly increased *WUS* expression as compared to wild type	[29,30]
ham mutant	*CLV3* expression is centered at in the lower middle region of the SAM	[13,33]
Induction of *CLV3* expression by 10-fold	Stable *WUS* expression pattern in the SAM	[34]

and the loss of both factors produced an even more dramatic increase (Fig. 2B, Indian red). Interestingly, the sum of the effects on *WUS* expression from the two single-mutants was less than the effect of the *erf-clv3* mutant (Fig. 2B, hatched vs. solid), suggesting a nonlinear cooperativity between EPFL and CLV3 signals. We found that this cooperativity was maintained when we perturbed the parameter values in the model (Fig. S2). Together with the observation that the loss of EPFL resulted in an increased CLV3 signal (Fig. 1E), our model further suggests that part of the lost inhibition of *WUS* expression in the *erf* mutant is compensated for by an increased level of CLV3. Together, these results show that EPFL and CLV3 signals synergistically control the lateral boundary of the *WUS*-expressing zone, whereas the apical-basal boundary of the *WUS*-expressing zone is primarily controlled by the CLV3 signal.

In addition to the synergy between EPFL and CLV3 in the regulation of *WUS*, we found that the spatial distributions of the cells producing EPFL and HAM (Fig. S1B and C) were critical for maintaining the expression patterns of both *WUS* and *CLV3*: the expansion of HAM production to upper layers resulted in the reduction of *CLV3* expression and the lateral expression of *WUS* expression; the expansion of EPFL to the middle SAM reduced the overall *CLV3* expression, and it dampened the *WUS* expression in the middle SAM while causing the lateral expansion of the *WUS* expression (Fig. S1B and C). These results suggest the synergy between EPFL and HAM, and the importance of their spatial distributions.

2.3. Inhibition of WUS and CLV3 expression by EPFL is important for maintaining SAM patterning

It was recently observed that EPFL inhibits the expression of both *WUS* and *CLV3* [29]. It was, however, unclear how each of these inhibitions contributes to SAM patterning. We therefore removed these two inhibitory relationships from our model one at a time and examined the steady state patterning of the SAM (Fig. 3). We found that upon the loss of *CLV3* inhibition by EPFL, there was a 30% increase of both *CLV3* mRNA and CLV3 protein in the SAM. Interestingly, *CLV3* was expressed around the organizing center in both the apical and lateral directions (Fig. 3A and C). This lateral expansion of *CLV3* expression suggests that the inhibition of *CLV3* by EPFL is critical for restricting *CLV3* expression in the top layers of the middle SAM. In addition, *WUS* expression moderately decreased compared to the wild type (Fig. 1C) due to the expanded *CLV3* expression. When we removed the inhibition of *WUS* by EPFL, the *WUS* expression region had a significant lateral expansion, and its expression in the middle region also increased compared to the wild type (Fig. 3B and C, dotted line). These analyses demonstrated the paradoxical roles of EPFL on *WUS* expression: it directly downregulates *WUS* in both the lateral and

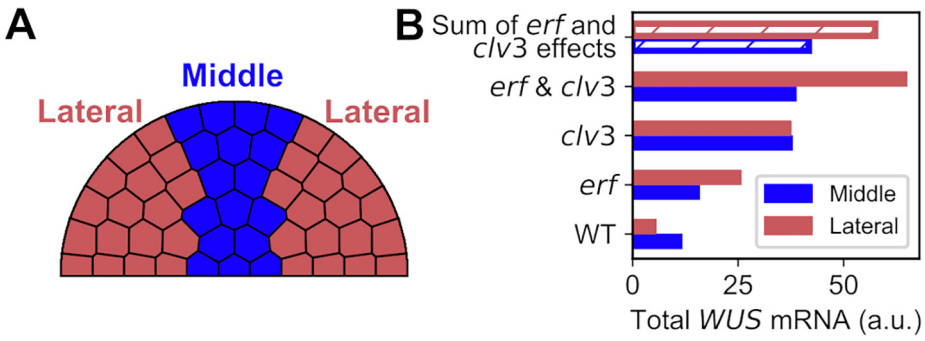

Fig. 2. EPFL and CLV3 control patterns of *WUS* expression at different regions. A. An illustration of two regions that were analyzed for *WUS* mRNA production. Region 1 (blue) contains cells near the apical-basal axis of the SAM, whereas Region 2 (Indian red) contains cells at the lateral boundary between the middle zone and the peripheral zone. B. Total *WUS* mRNA in the two regions indicated in A. Simulations were performed with the model structure described in Fig. 1. Mutant genotypes were modeled by removing the production of the indicated mRNAs. The hatched bars were calculated by adding the amounts of mRNA in the *erf* mutant and *clv3* mutant increased from wild type, and the amount of wild-type mRNA. (For interpretation of the references to color in this figure legend, the reader is referred to the web version of this article.)

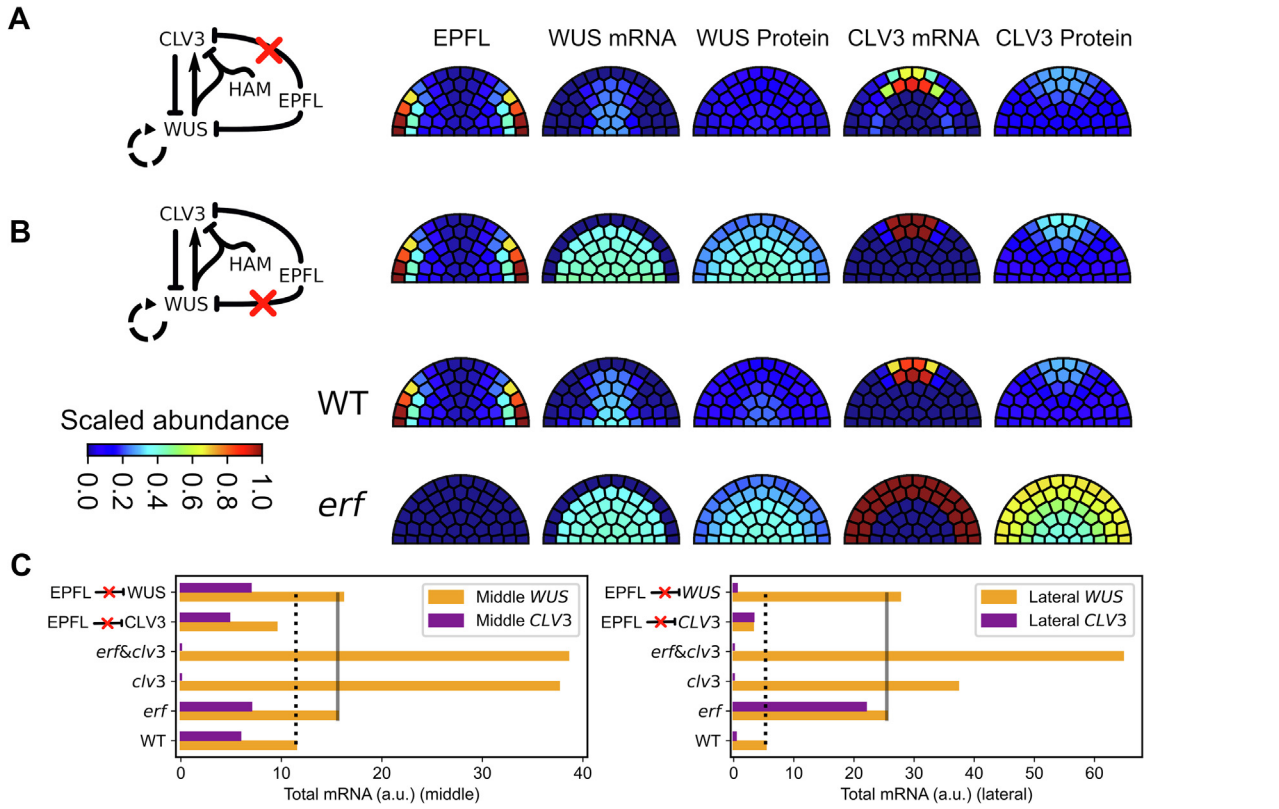

Fig. 3. The effects of WUS and CLV3 inhibition by EPFL. A. A simulation with the removal of *CLV3* inhibition by EPFL. B. A simulation with the removal of *WUS* inhibition by EPFL. In both A and B, the indicated transcriptional inhibition was removed from the model by increasing the threshold to a large number (1000). Simulations were performed with the procedure as those described in Fig. 1. Steady state SAM patterns were analyzed. Wild type and *erf* mutant patterning are shown for comparison. C. Left: *WUS* and *CLV3* mRNA in the middle region (Fig. 2, blue). Right: *WUS* and *CLV3* mRNA in the lateral region (Fig. 2, Indian red). Dotted lines are visual guides for wild-type *WUS* mRNA. Gray lines are visual guides for *erf* mutant *WUS* mRNA. (For interpretation of the references to color in this figure legend, the reader is referred to the web version of this article.)

middle regions of the SAM while it indirectly upregulates the same gene by inhibiting *CLV3*. The direct downregulation has the dominant effect, because blocking this regulation produced a *WUS* pattern similar to that of the *erf* mutant (Fig. 3, gray line). Nonetheless, the slightly higher *WUS* expression in the blocked EPFL-to-*WUS* condition than in the *erf* mutant provides further evidence for the paradoxical roles of EPFL (Fig. 3, gray line). Together, these results show that EPFL inhibition of both *WUS* and *CLV3* is critical for SAM patterning.

We found that the alterations of the gene expression upon perturbations were not always intuitive. For example, blocking the EPFL-to-*CLV3* inhibition resulted in a reduction of *CLV3* mRNA in the middle of the SAM (Fig. 3C), suggesting the importance of the negative feedback loop between CLV3 and WUS. In the next section, we describe our analyses of the interconnected feedback loops in the SAM.

2.4. Paradoxical feedbacks between WUS and CLV3 maintain robust patterning in apical-basal axis of SAM

We noticed that the SAM regulatory network contains two feedback loops between WUS and CLV3 (Fig. 1A and Fig. 4A). In the first network motif, WUS activates *CLV3* expression and CLV3 inhibits *WUS* expression, forming a negative feedback loop. The second motif consists of *WUS* inhibition by CLV3, and *CLV3* inhibition by HAM and high concentration of WUS [13–15]. This motif is a double-negative (positive) feedback loop (Fig. 4A, top panel). These two feedback loops are both interconnected (i.e. they share a regulation) and paradoxical (i.e. they are negative and positive respectively). While the first loop is a well-known negative feedback that has been proposed to be critical for maintaining the homeostasis of the SAM, the function of the interconnected and paradoxical feedbacks between WUS and CLV3 is unclear. To examine the roles of these two feedbacks on SAM patterning, we constructed two alternative models with disrupted negative and positive feedbacks respectively (NFL-KO, PFL-KO models. Fig. 4A). For NFL-KO model, we introduced a hypothetical activation signal for CLV3 in the L1 and L2 layers of the central zone. This signal avoids the trivial outcome of the complete absence of CLV3 in the SAM, and the addition of the signal gave rise to a SAM pattern similar to the wild type (Fig. 4B). For the PFL-KO model, we removed the downregulation of *CLV3* by the WUS signal. In order to compare these alternative models to the basal (wild-type) model in terms of *WUS* expression patterning, we further adjusted the synthesis rate constants of *CLV3* mRNA in the alternative models such that the overall *WUS* expression patterns obtained with the three models are comparable (Fig. 4B).

We next perturbed the expression of *WUS* by reducing its mRNA synthesis rate constant. This perturbation reflects possible aberrant environmental or genetic changes. Because the regulation of *WUS* itself was not altered in the PFL-KO or NFL-KO models, this perturbation was not biased towards any model in a trivial way. However, the wild type model was robust with respect to the perturbation in terms of total WUS production in the SAM (Fig. 4C): a 50% decrease of the rate constant resulted in less than 10% loss of the *WUS* in the wild type SAM (Fig. 4C, orange). In contrast, the loss of either negative or positive feedback decreased the stability of *WUS* production when challenged with the same perturbations. In particular, the NFL-KO model had a more prominent decrease of *WUS* production (>3-fold from unperturbed condition) than

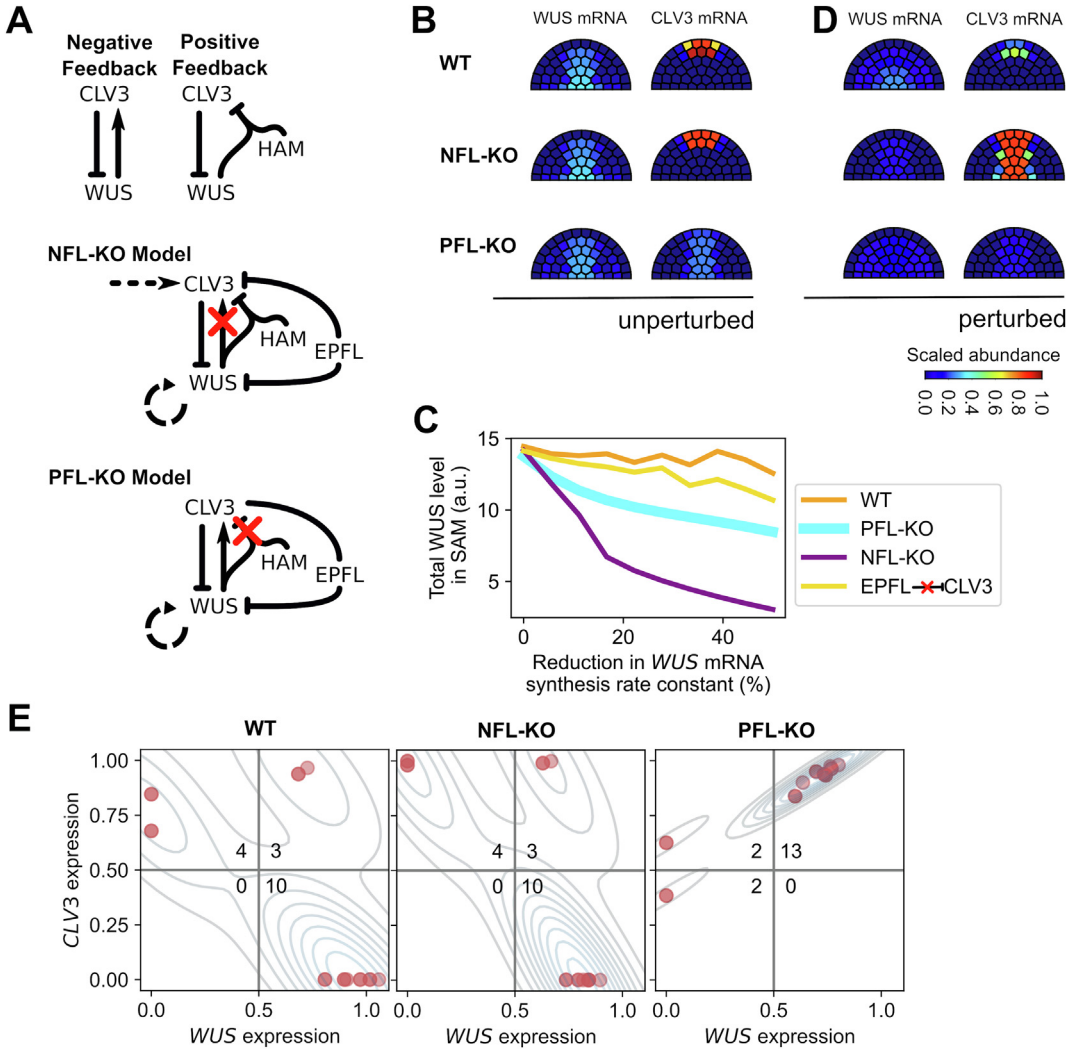

Fig. 4. Roles of paradoxical feedbacks between WUS and CLV3. A. Top: two motifs showing the negative and the positive feedback between WUS and CLV3. Middle: network structure of negative feedback knockout model (NFL-KO) which does not have a WUS-CLV3 negative feedback loop. Dashed line indicates a hypothetical activation signal for maintaining CLV3. Bottom: network structure of positive feedback knockout model (PFL-KO) which does not have the WUS-CLV3 positive feedback loop. B. Steady state distributions of *WUS* and *CLV3* mRNA in SAM with circuits of wild-type, NFL-KO and PFL-KO models. C. Steady state distributions of *WUS* and *CLV3* mRNA in SAM with circuits of wild-type, NFL-KO and PFL-KO models with 50% reduction of *WUS* mRNA production rate constant. D. Total *WUS* mRNA in SAM with respect to reduction of *WUS* mRNA production rate constant. E. Distributions of 17 middle SAM cells in the phase space of *WUS* and *CLV3* mRNA with three models under normal condition. Each dot indicates a cell and in the middle region of the SAM (Fig. 2A Indian red), and its coordinates show the levels of *WUS* mRNA and *CLV3* mRNA, respectively. Contour maps show the density of these cells in the *WUS* and *CLV3* mRNA space. Numbers in quadrants indicate cell numbers. The cell numbers in the top left and lower right quadrants reflect the diversity of the WUS^{on} and $CLV3^{on}$ cells. (For interpretation of the references to color in this figure legend, the reader is referred to the web version of this article.)

the PFL-KO model did (Fig. 4C, purple), suggesting that the negative feedback has a dominant role in protecting the stability of *WUS* production in the SAM. In earlier analysis, we showed that blocking the inhibition of *CLV3* by EPFL gave rise to a *WUS* expression pattern comparable to the wild type (Fig. 3A), a feature found in the NFL-KO and PFL-KO models. We observed that the inhibition of *CLV3* by EPFL also facilitates the maintenance of *WUS* expression stability, but its effect is less than that of the feedback loops (Fig. 4C, yellow). We found that when the *WUS* mRNA production rate constant was reduced in the wild type, the level of *CLV3* expression was significantly decreased (Fig. 4D), which in turn compensated for the loss of *WUS* mRNA production, thereby maintaining the stability of *WUS* expression in the SAM via a negative feedback. This compensation effect via downregulation of *CLV3* was not observed with the NFL-KO model, and was only moderate in the PFL-KO model as compared to the wild type model (Fig. 4D). We further perturbed the system with increasing WUS production rate constant, and we used additional metrics to examine the response in terms of the SAM patterning. We found that the wild-type model consistently performed equally well as or better than the alternative models (Fig. S3).

Positive feedback (or double-negative feedback) is widely used in developmental systems for maintaining tissue boundaries [35,36]. In the wild type SAM, cells along the middle apical-basal axis are either $WUS^{off}CLV3^{on}$ or $WUS^{on}CLV3^{off}$ except for L2 cells which had significant expression of both *WUS* and *CLV3* (Fig. 4B and E). The robustness of the anticorrelated expression pattern of *WUS* and *CLV3* in most cells of the SAM was also reflected in mutant simulations when EPFL-driven inhibition was partially or completely lost (Fig. 1E, 3, and 4B). However, in the absence of the positive feedback loop (Fig. 4A, PFL-KO model), the number of cells co-expressing *WUS* and *CLV3* increased significantly, and the anticorrelation pattern of *WUS* and *CLV3* expressions was lost (Fig. 4B and E).

Together, these results show that the paradoxical feedbacks between WUS and CLV3 are critical both for stabilizing *WUS*

expression and for generating the separation between *WUS*-expressing and *CLV3*-expressing regions. Stable *WUS* expression may be important for maintaining the size of the SAM, while separation between *WUS*-expressing and *CLV3*-expressing cells may be important for maintaining diverse cellular properties, such as proliferation rate, in different regions of the SAM [23]. The specialization of cellular phenotypes along the apical basal axis may in turn support the robust structure of the SAM.

2.5. Tradeoff in maintaining SAM patterning

Due to the lack of quantitative measurement in terms of the SAM patterning, we did not attempt to obtain a single parameter set that gives the best fit to experimental data in this study. However, the emergence of the simulated SAM patterns that are qualitatively consistent with many experimental observations allows us to interrogate the influence of the parameter values on the SAM patterning in a collective manner. In the previous sections we discussed three key features of the SAM regulatory network: 1) the network uses two signals to fully repress *WUS* expression in the lateral region of the SAM; 2) the network maintains the stability of WUS production in the SAM using two feedback loops; and 3) the network generates a distinct populations containing WUS^{on} cells and $CLV3^{on}$ cells in the middle region of the SAM. If these three features are critical for plant physiology, how would the kinetic rate constants of the system be optimized to achieve them? To gain insight into this question, we used three metrics describing three performance objectives: lowering *WUS* expression in the lateral region, lowering the variability of *WUS* production in the presence of perturbations, and increasing the number of WUS^{on} cells and $CLV3^{on}$ cells in the middle region (Fig. 5A). For easier interpretation, all three metrics were designed such that lower scores mean 'better' performance and higher scores mean 'poorer' performance (see Methods, Fig. 5B top). We perturbed 23 model parameters by decreasing each of them 2-fold, and then increasing each 2-fold, scored the performance of the perturbed models using the three performance metrics, and then normalized them to the scores obtained from wild type model (Fig. 5B) by subtracting the wild-type scores from the scores of the perturbed models (see Methods). Among the three metrics, the scores of the diversity metric (Metric III) were most robust with respect to the perturbations among the three metrics, possibility because it is based on a discrete measurement in terms of cell numbers rather than a continuous one. Changes in each parameter had some influence on at least one performance score, and changes in 13 out of the 23 parameters had one performance score better than the basal one. However, none of the changes of individual parameters gave rise to better performance in two or three metrics (Fig. 5, heatmap, Fig. S4).

This analysis suggests a possible tradeoff in optimizing the kinetics of the SAM network: achieving better performance in one metric is likely accompanied with jeopardized performance in at least one other metric. However, this phenomenon might be simply due to the fact the very few perturbations of individual parameters had improved performance in any metric, so the absence of better performance in two or three metrics may just occur by chance. To further examine the relationship among these three performance objectives, we generated 10^4 perturbed models with all of their parameter values deviated from the basal set. These parameter values were randomly selected from intervals bounded by values with 50% changes from the basal set. Among these 10^4 randomly perturbed models, 1964 of them had improved performance score (less than 0, or better-than-basal) for Metric I, 202 of them had improved score for Metric II and 423 of them had improved score for Metric III (Fig. 6A). However, only 2 of them had improved scores for all three metrics. We performed a permutation test and confirmed that this number is significantly low (Fig. 6B, upper panel, $p < 10^{-4}$). Furthermore, when a model had a better-than-basal score in one or more metric, the probability that it also had a lower-than-basal score in one or more metric was 99.8%, a number that is significantly higher than expected (Fig. 6B, lower panel, $p = 0.006$). These results show that there exists a tradeoff in optimizing the three performance objectives of SAM patterning. We then asked which pairs of metrics have a significant tradeoff problem when multiple kinetic rate constants are varied, and we found that if a model has a better score for Metric I or Metric II (lateral inhibition and stability), there is a significantly high probability that it has a poorer score for Metric III (divergence), suggesting that there is a pairwise tradeoff between optimizing for *WUS-CLV3* diversity and other features (Fig. 6C). Other pairs of metrics did not show significantly high probability of having such opposite trends of performance change (Fig. 6C). Overall, these results suggest that there may exist a tradeoff among the three objectives of the SAM patterning when the system varies its rate constants to achieve those goals simultaneously.

3. Discussion

3.1. Two-axis control of WUS expression in the SAM

Patterning of *WUS* and *CLV3* expression in the SAM is considered to be a crucial system for stem cell maintenance in plants. In this study, we built a multicellular model describing the key gene regulatory network controlling SAM patterning. In particular, we considered signals that regulate *WUS* expression from both the middle SAM and peripheral regions. This differs from previous models which focused on the middle SAM region around the apical-basal axis [11,13,16–18,22–25]. Our model shows how the system combines the peripheral signal EPFL with the CLV3 signal originating from the top central SAM to restrict *WUS* expression to the organizing center in the meristem rib. In addition, this peripheral signal synergizes with the WUS and HAM signals from the meristem rib to restrict *CLV3* expression to the top central SAM. Notably, this localization of *CLV3* expression can be achieved without assuming pocket-like expression regions of any inhibitory factor [13,22]. The prominent roles of EPFL in regulating SAM patterning by modulating *WUS* and *CLV3* expression is consistent with its key roles in plant development that were identified previously [28–30]. The model reveals a remarkable cooperativity of the peripheral and middle signals for shaping the patterning of *WUS* and *CLV3* expression. This cooperativity is particularly manifested in our observation that *WUS* expression in the lateral SAM region is controlled by both CLV3 and EPFL, each of which has partial but significant impact on *WUS* inhibition. Our results suggest that stem cell maintenance in *Arabidopsis* requires a highly regulated crosstalk between the middle and peripheral regions of the SAM rather than signals in the middle apical-basal axis alone.

3.2. Patterning and size regulation of the SAM and model limitations

Our modeling study focuses on gene expression patterning, which has a major influence on the size of the SAM. Because of the central role of WUS in maintaining the stem cell population and its positive correlation with cell proliferation rates, it is reasonable to use changes in the amount of WUS in the SAM as an indicator for changes in SAM size. For example, upregulation of *WUS* that was observed in *erf*, *clv3* and other mutants is expected to correlate with an increase of stem cell populations, which in turn gives rise to an increase in SAM size. This is consistent with previous experimental observations under such conditions [29,32,37–39]. However, the interplay between cell proliferation and gene expression patterning is bidirectional, dynamic, and more complex

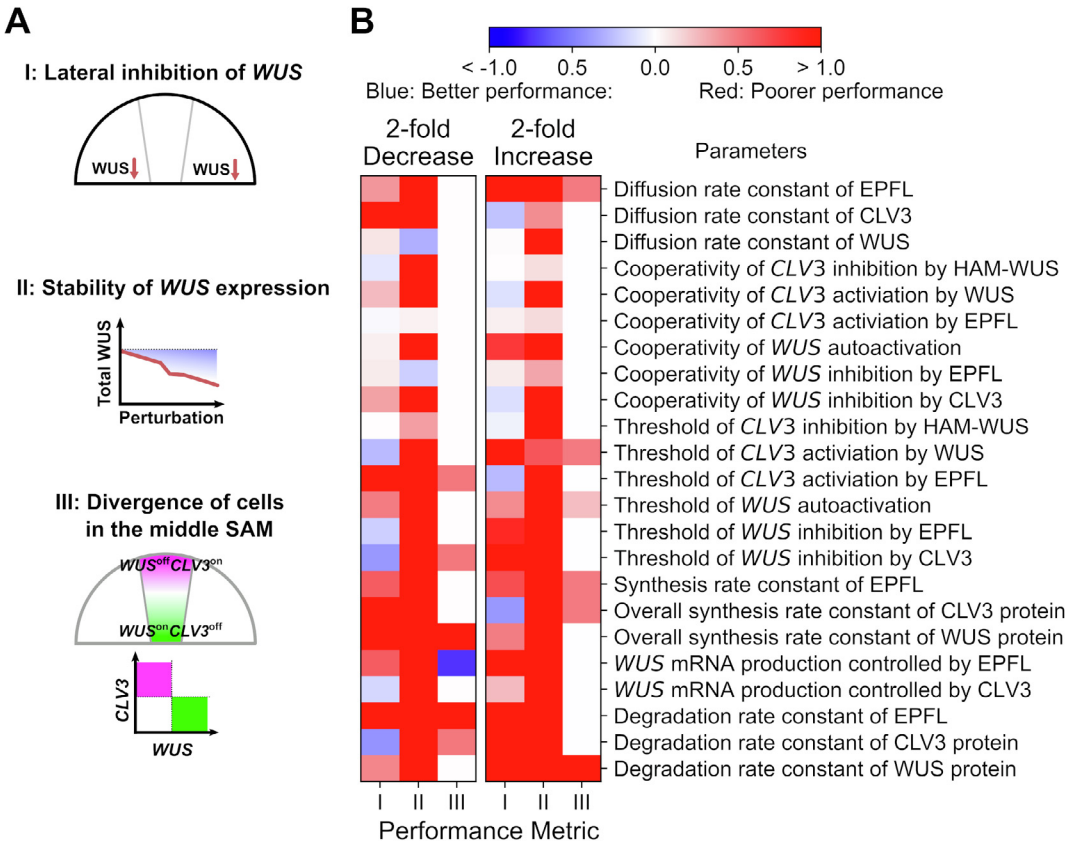

Fig. 5. Influence of parametric changes on three performance objectives of SAM patterning. A. Illustrations of the three performance metrics of SAM patterning. See Methods for details of these metrics. B. The performance scores upon perturbations of 23 parameters. Each parameter was decreased and increased by 2-fold and simulation was performed in the same procedure as that with the wild-type (basal) model. Steady state SAM patterning was scored based on the three metrics, and the scores were compared with those obtained with basal model. Blue: perturbed model has better score than basal model does. Red: perturbed model has poorer score than basal model does. White: perturbed model and basal model have the same score. (For interpretation of the references to color in this figure legend, the reader is referred to the web version of this article.)

than this simple inference assumes. For example, lateral expansion of the SAM during development could in theory reduce the effect of EPFL on the middle region unless the production rate of EPFL scales with the expansion. Understanding these forms of interplay will be important for quantitative characterization of SAM patterning and size control. Furthermore, it has been shown that the size and the shape of the SAM undergo significant changes in processes such as ontogeny [40], suggesting the complexity of the size-patterning interplay. Finally, cytokinin and auxin hormones, transcription factor SHOOTMERISTEMLESS (STM), microRNAs and other CLE peptides may influence meristem patterning directly, by regulating the rate of cell proliferation, or by interacting with the WUS-CLV3 loop [41–48]. Ultimately, these regulators also need to be incorporated into the model of SAM regulation once their role in the SAM and the interplay with the WUS-CLV3 loop are clearly defined. Nonetheless, our work provides critical insights into the middle-peripheral interplay of SAM patterning, which can serve as a foundation for future development of more complex and more realistic models of SAM growth.

3.3. The roles of paradoxical feedbacks

It has been long considered that the negative feedback between *WUS* and *CLV3* plays an essential role in maintaining the stem cell population in the SAM [9,10]. The self-limiting property of negative feedback ensures the stable expression of both genes. However, recent data suggest that the interactions between *WUS* and *CLV3* might be more complex than a negative feedback loop: WUS and HAM from the meristem rib can inhibit *CLV3*, which is prevented from being expressed below the subepidermal layer [13–15,49]. As such, WUS and CLV3 are involved in a negative feedback loop as well as a positive (or double-negative) feedback loop. The latter network motif is known for its function in generating switch-like behaviors and formation of tissue boundaries during development [50,51]. Consistent with these features, we found that this interconnected, paradoxical feedback WUS-CLV3 network supports the stability of WUS expression against alteration of kinetic rates, and it facilitates the diversification of SAM cells, in particular cells in the middle region, into WUS^{on} and $CLV3^{on}$ cells. Although the two types of cells do not have a clear boundary along the apical-basal axis at single cell-layer resolution, the formation of a heterogeneous population with stable phenotypic composition is consistent with established theories about positive feedback loops [52].

Since the homeostatic function of a negative feedback loop does not necessarily depend on the spatial separation of two types of molecules, why does the SAM need to separate WUS^{on} and $CLV3^{on}$ cells? One plausible reason is that the stem cell transcriptional program depends on a high concentration of CLV3 and a low concentration of WUS. Another possibility is that the differential cell proliferation rates along the apical-basal axis [23], which can be governed by heterogeneous expression patterns of *WUS* and *CLV3*, may play essential roles in maintaining the structure of the SAM. Future work is warranted to connect these molecular and cellular features of SAM patterning to the physiology of plants.

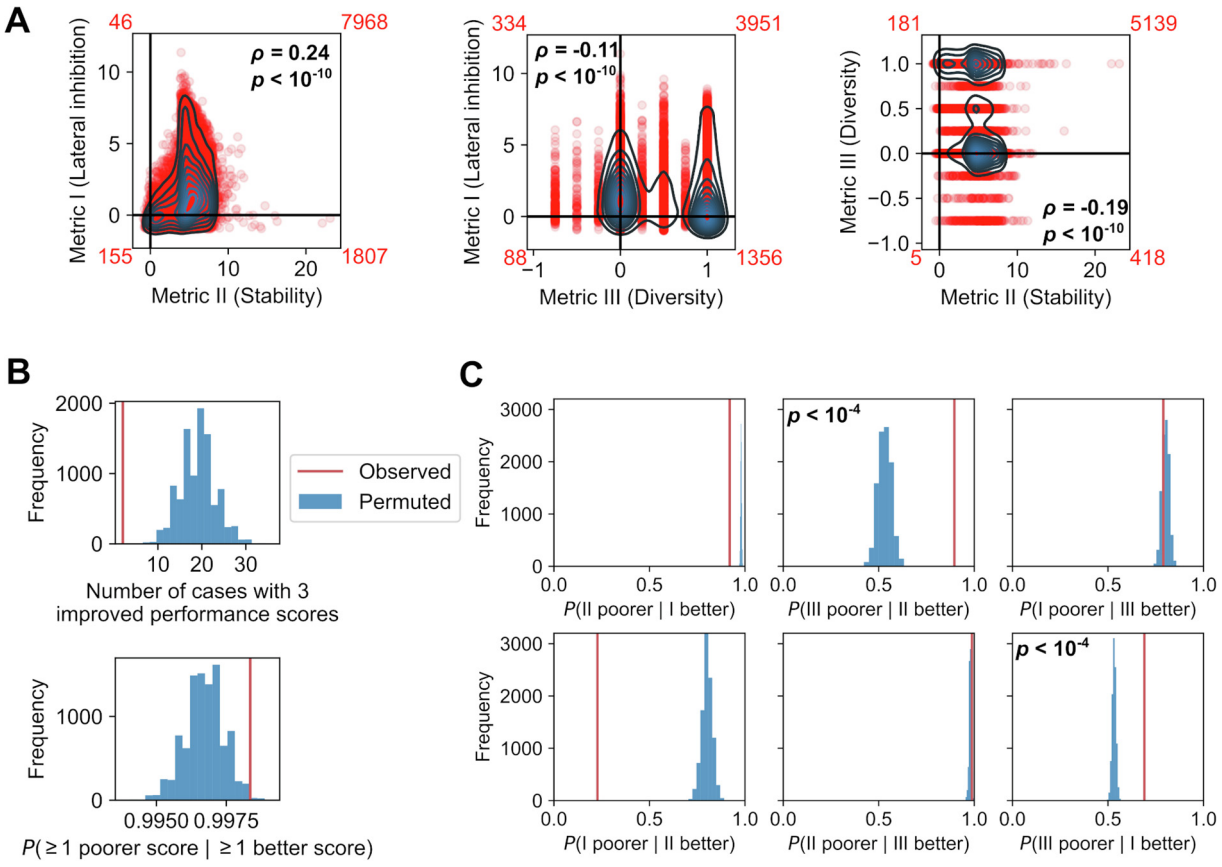

Fig. 6. Tradeoffs in optimizing parameters to gain better performance of SAM patterning. 10,000 models were generated with random parameter values around those of the basal (wild-type) model. These values were chosen from a uniform distribution bounded by ±50% from the corresponding basal values in the wild-type model. Each model was simulated in the same way as with the basal model, and then the steady state SAM patterning was scored with the three metrics mentioned in Fig. 5 (see Methods for details). Positive scores mean poorer performance than wild-type model. Negative scores mean better performance than wild-type model. A. Score distributions in phase space of all pairs of metrics. Red numbers show cases in quadrants, e.g. numbers for the lower left quadrants show the numbers of models with improved scores from basal model in two metrics. Models with scores on the x or y axis were not included in red numbers. Spearman correlation coefficient and its *p*-value are shown in each panel. B. The scores of the perturbed models were arranged in a 10,000 × 3 matrix. Each of the three columns were randomly permutated 10,000 times independently, and the resulting 10,000 matrices were analyzed based on statistics of their rows. Blue: histogram of scores or probabilities with permuted scores. Red: Observed scores or probabilities with the perturbed models. Top panel shows the cases with three better (improved) scores (there are two observed cases out of the 10,000). Lower panels show the probability of obtaining at least one poorer score under the condition of obtaining at least one better score. C. Pairwise conditional probabilities of obtaining opposite performance in two metrics. The right-tail *p*-value is >0.05 unless otherwise indicated. (For interpretation of the references to color in this figure legend, the reader is referred to the web version of this article.)

3.4. Tradeoffs in optimizing the SAM gene regulatory network

Tradeoffs in designing biological circuits have been extensively studied previously; e.g., the tradeoff between noise attenuation and speed of response, and that between maximizing information content in individual cells and cell populations [53,54]. However, the roles of tradeoffs in complex traits such as tissue patterning remain elusive. Although the exact physiological function of SAM patterning is only partially understood, it is clear that the structure of the SAM gene regulatory network and its underlying biochemical properties serve multiple purposes, because diverse alterations of SAM patterning are often associated with abnormal development ranging from organ formation failure to nonoptimal size of organisms [6,7,28,33]. Our modeling study revealed that the kinetic rates in the SAM gene regulatory network have a general tradeoff among achieving multiple 'desired' features of patterning. For example, parameter sets that can achieve more diverse populations of *WUS*^{on} and *CLV3*^{on} cells are likely associated with less stability in terms of *WUS* expression, or less regulation of *WUS* expression in the lateral region. These nontrivial tradeoffs may act as a complex selection pressure similar to multi-objective optimization problems, and they can play crucial roles in shaping the structure and kinetic rates of the SAM regulatory network through evolution. Furthermore, while there are a wide variety of SAM regulations in plants and a single optimal set of biochemical kinetic rate constants may not exist even within a single species, the tradeoff among the goals may serve as a general principle in shaping these kinetic rate constants.

Overall, our model includes a few key elements for controlling SAM patterning that were not considered previously. It captures many patterning phenotypes observed under normal conditions and with genetic perturbations. It offers insights into the interplay between peripheral and middle SAM signals, the intricate feedback regulations, and the principles governing the network design of this system.

3.5. Resource availability

Computer code for reproducing all key results and figures is available at: https://github.com/lfsc507/sam

4. Methods

4.1. Construction of mathematical model

To model the spatiotemporal dynamics of gene regulation in the shoot apical meristem (SAM), we considered 51 cells that are organized in a dome-like structure. We estimated this number of cells in the SAM from Chen et al. [38], and a similar number was used in a recent SAM model [13]. We described this 2D cellular network with 51 points within a half-circle with a radius of 25 μm [38]. In the model, the diffusive EPFL ligands are synthesized in the peripheral regions distant from the middle apical-basal axis and inhibit the expression of both *WUS* and *CLV3* through binding to their receptors which are assumed to be broadly expressed in the SAM [28,29]. CLV3 is a diffusive peptide, and WUS is a transcription factor that moves across cells [11,55,56]. In addition to the WUS-CLV3 negative feedback and these lateral regulators, our model describes a HAIRY MERISTEM (HAM) signal that originates from the rib zone and inhibits *CLV3* expression in the organizing center [13]. In this model, we do not assume that HAM can move across cells due to the lack of experimental evidence. The spatial distribution of *HAM* expression is established by a diffusive microRNA that is not considered in the model explicitly [46]. It has been shown that HAM and WUS control gene expression synergistically [49], and that high concentration of WUS may also contribute to *CLV3* downregulation [14,15]. We therefore assumed that the inhibition of *CLV3* expression by HAM signal depends on WUS. As such, WUS has a paradoxical role (both activation and inhibition) in regulating *CLV3* in the presence of HAM. Finally, we considered a CLV3 independent positive feedback involving WUS. This feedback may be supported by a WUS-cytokinin mutual activation loop: it was previously shown that cytokinin activates *WUS* expression [23,39,57], whereas WUS derepresses cytokinin signal by inhibiting Type A *ARABIDOPSIS RESPONSE REGULATOR* (ARR) genes which act as inhibitors of cytokinin [14,58,59]. In addition, the WUS autoactivation loop may be supported by other factors [27]. Based on these assumptions, dynamics of six interacting species representing concentrations of regulatory molecules is described with nonlinear ordinary differential equations (ODEs) in each cell (point) of the model (additional spatial constraints are shown in Fig. 1B):

$$\frac{dW_p}{dt} = k_{W_p} W_r - b_W W_p + D_W \Delta W_p \tag{1a}$$

$$\frac{dC_p}{dt} = k_{C_p} C_r - b_C C_p + D_C \Delta C_p \tag{1b}$$

$$\frac{dW_r}{dt} = k_{W_r}\left(\frac{k_{WL}}{1+\left(\frac{L}{K_{WL}}\right)^{n_{WL}}} + \frac{k_{WC}}{1+\left(\frac{C_p}{K_{WC}}\right)^{n_{WC}}}\right)\left(k_{0W} + \frac{\left(\frac{W_p}{K_{WW}}\right)^{n_{WW}}}{1+\left(\frac{W_p}{K_{WW}}\right)^{n_{WW}}}\right) - b_{W_r} W_r \tag{1c}$$

$$\frac{dC_r}{dt} = \frac{k_{C_r}}{1+\left(\frac{L}{K_{CL}}\right)^{n_{CL}}}\left(a_C + \frac{\left(\frac{W_p}{K_{CW}}\right)^{n_{CW}}}{1+\left(\frac{W_p}{K_{CW}}\right)^{n_{CW}}}\right)\frac{1}{1+\left(\frac{H}{K_{CH}}\right)^{n_{CH}}} - b_{C_r} C_r \tag{1d}$$

$$\frac{dL}{dt} = k_L - b_L L + D_L \Delta L \tag{1e}$$

$$\frac{dH_p}{dt} = k_P - b_P H_p \tag{1f}$$

here, state variables W_r, W_p, C_r, C_p, L and H_p represent the concentrations (or strengths) of *WUS* mRNA, WUS protein, *CLV3* mRNA, CLV3 protein, EPFL, and HAM respectively. H represents a meristem rib signal that combines both HAM and WUS, the latter of which inhibits *CLV3* expression at high concentration. A full list of parameter descriptions and their numerical values is available in Table S1. Briefly, k_X is the production rate constant of molecule X; b_X is the degradation rate constant of molecule X; K_{XY} is the threshold of activation or inhibition of X by Y. n_{XY} is the cooperativity of activation or inhibition of X by Y; D_X is the rate constant of passive diffusion-like transport of molecule X; Δ is the Laplace operator describing gradients of concentrations, which govern passive diffusion-like transport; ΔX has a unit of concentration per unit area. D_X was adjusted by multiplying with a scaling factor $\langle l \rangle / l$, where l represents the distance between the centers of the two cells [60]; and neighboring cells are defined as cells that are located within a radius of 10 μm. We neglected the subcellular geometry of the cells, their contact areas and the influence of mechanics in this study (the effected contact area for WUS transport cannot be directly inferred from total contact area of plasma membrane) [13]. The diffusion of EPFL and CLV3, and the diffusion-like symplastic transport of WUS are responsible for the intercellular communication in the model. We used Hill function to describe nonlinearity in the gene regulation. Previous models of the SAM and other complex systems have used similar nonlinear functions [17,19,22,61]. a_C is a constant for us perturb the negative feedback regulation (see next section). When a molecule is controlled by multiple factors, we assumed a multiplicative form of Hill functions (AND-gate-like) (for example, nonlinear interaction of WUS and HAM may arise from their physical interactions [49]), except for the inhibitions of *WUS* by CLV3 and EPFL, which were assumed to be additive (OR-gate-like). Because the absolute concentrations of these molecules have not been measured experimentally, we used an arbitrary unit (a.u.) to describe concentration (or strength) of each molecule. Once these measurements become available, one can easily scale these variables to fit to specific concentrations. We used no-flux boundary condition for the model, and this is similar to a recently published SAM model [13].

We fit the parameters to known patterning phenotypes of the SAM under normal and genetically perturbed conditions (see details of mutant models below). These phenotypes are listed in Table 1. Because only qualitative information is available from the experimental data, we performed the fitting manually. Here, we do not attempt to obtain an optimal set of parameters that give the best fit to experimental data. We instead discuss the general trends of the influence of each parameter on multiple features of the SAM patterning (see Performance Metrics). To perform a simulation for a SAM system, we solved the system of ODEs numerically using the Tellurium package [62]. The initial concentrations for all variables were set to zero. An example of the time course solution of the wild type SAM is shown in Movie S1. For all our analyses, steady state solutions (at Day 100) were used to determine the patterning of the SAM.

4.2. Simulations for mutants

For each mutant SAM model, we simulated the genetic perturbation by setting the production rate constant for the knocked-out gene(s) to zero. These parameters include k_{W_r} for the *wus* mutant, k_{C_r} for the *clv3* mutant, k_L for the *erf* mutant, and k_H for the *ham* mutant.

To examine the roles of individual interactions in the gene regulatory network, e.g. the activation of *CLV3* by EPFL, we set the parameters describing the activation/inhibition thresholds (K) of the interactions to 1000 a.u., which exceeds the maximum concentrations of the activators/inhibitors.

All other parameters were kept the same as those in the wild-type model. Steady state distributions of all modeled molecules were obtained with the same procedure as the simulation for the wild-type SAM.

4.3. Normalization of concentrations for visualization

All analyses of molecular abundance (concentrations) were based on raw values obtained from the simulations. However, because visualization of the SAM patterning with multiple molecules would involve using the same color scale (jet colormap) for different ranges of concentrations, we normalized the concentrations of all molecules by dividing all values by their own maximum concentration across all genotypes before visualization. Therefore, the ranges of all visualized abundance are [0, 1], where the value 1 effectively represents the maximum concentrations of individual molecules across all simulations.

4.4. Models without feedback loops

To examine the roles of feedback loops on SAM patterning, we created two alternative models, each of which has a feedback loop (negative or positive) removed from the basal (wild type) model. To 'knockout' a feedback loop, we first removed the regulation of *CLV3* by either the WUS or HAM signal by setting threshold constants (K) to 1000 a.u.. The removal of these interactions generates prominent changes of SAM patterning. For example, if WUS-to-*CLV3* inhibition is removed from the basal model, then *CLV3* is not expressed in the SAM and *WUS* is highly expressed compared to the basal model. However, these changes may not reflect the fitness advantage of the feedback loop because the other kinetic rate constants can be altered to compensate for the effect of the removal of the interactions. We therefore further adjusted the parameters to mimic this compensation. For the negative feedback knockout model, we introduced an activation signal for CLV3 by letting $a_c = 1$, reducing k_{C_r} by 15%, and reducing k_{W_r} by 50%. With this adjustment, the *WUS* expression pattern became comparable to the wild type. For the positive feedback knockout model, we reduced k_{C_r} by 85% and reduced k_{W_r} by 50%. The *WUS* expression pattern with this model also became comparable to the wild type. After these changes, we compared the feedback knockout models with the basal model in terms of *WUS* expression patterning in similar dynamic ranges.

4.5. Performance metrics for SAM patterning

To quantify the effect of changes in parameter values on SAM patterning, we used three performance metrics. These metrics are used to describe traits that might be critical for normal plant physiology rather than fit to experimental data, which are not available in a quantitative manner in most studies of SAM patterning. We do not claim that plants optimize their biochemical rate constants to achieve these three goals in general, because there are many other objectives that plants must achieve to gain better fitness. Our focus is rather on the relationship among these three goals.

Metric I (lateral inhibition) describes the ability of the system to inhibit *WUS* expression in the lateral region of the SAM. Specifically, it is the total *WUS* mRNA at steady state in 34 cells that are closest to the peripheral boundaries, i.e.

$$M_1 = \sum_i^l w_i \tag{2}$$

where l is the total number of cells in the lateral region (34), and w_i is the steady state WUS mRNA concentration in cell i.

Metric II (WUS stability) measures the deviations of total WUS in the SAM from unperturbed models to perturbed models when the mRNA production rate constant k_{W_r} is reduced by 0–50%. We chose 10 levels of such reduction in the parameter in the interval [0, 0.5], and obtained the deviation score given by:

$$M_2 = \sum_i^m \sum_j^n \left| W_{i,j} - W_j^0 \right| \tag{3}$$

where m is the number of perturbations (10), n is the number of cells the SAM (51), and $W_{i,j}$ is the steady state level of WUS protein in cell j with perturbation i, and W_j^0 is the steady state level of WUS protein in cell j with the unperturbed parameter set.

Metric III (*WUS-CLV3* heterogeneity) describes the size and heterogeneity of the cell population consisting of $WUS^{on}CLV3^{off}$ and $WUS^{off}CLV3^{on}$ cells in the middle region of the SAM. First, the *WUS* and *CLV3* expression was binarized with a threshold of 0.5 a. u.. Next, we calculated the heterogeneity score with the following function:

$M_3 = |x - y| - (x + y)$ (4)where x is the total number of WUS^{on}-$CLV3^{off}$ cells in the middle region (17 cells closest to the central axis) of the SAM, and y is the total number of $WUS^{off}CLV3^{on}$ cells in the same region.

The scores of the basal (wild type) model are 5.3, 0.48 and −8 for M_1, M_2 and M_3 respectively. We perturbed the parameters in the basal model in two ways and then examined the performance of the perturbed models (note that this perturbation is different from that in Metric II). In the first analysis, we decreased each parameter of the model by 2-fold, and then increased it by 2-fold. These two perturbations were performed for each parameter and six scores were obtained. In the second analysis, we perturbed all parameters in the model by randomly selecting their values from the intervals $[u/2, 3u/2]$, where u is the basal value of each parameter. These parametric changes represent the alterations of biochemical rate constants that may occur through evolution to achieve desired fitness goals.

Since we are interested in how these performance scores (M_1, M_2 and M_3) change when the parameters of the model are systematically perturbed from the basal set, we further normalized the raw values of these scores with the performance score obtained from the basal parameter, i.e.

$$m = \frac{M - M^0}{\left| M^0 \right|} \tag{5}$$

where M is the performance score of the perturbed model, and M^0 is the performance score of the basal model. The same normalization was used to scale the scores for all three metrics. As such, if the perturbation gives rise to a performance better than that obtained with the basal set, the normalized score is negative. If the performance is poorer than that with that obtained with the basal set, the normalized score is positive.

4.6. Permutation test

The parametric perturbations and performance scoring described in the previous section generate performance scores that can be organized in an $n \times 3$ matrix, where n is the number of perturbations. In our random perturbation of parameters, the value of n is 10^4. We are interested in whether there exists a significant tradeoff in obtaining better scores of all three metrics when multiple parameters are perturbed. We first described a possible tradeoff in a small number of cases in which all three performance scores are improved ($m < 0$) in these n perturbations. Out of the 10^4 parametric perturbations, only 2 of them gave rise to three negative scores. To test whether this number is significantly low, given that the total numbers of improved (better than basal) scores for the three metrics are 1964, 2020 and 423, respectively, we permutated each column of the matrix independently for 10^4 times. We next compared the distribution of the numbers of cases in which all three performance scores are improved in these 10^4 matrices with the observed

number of cases (2), and we calculated the empirical *p*-value with the area of the left-tail of the distribution with the right bound of 2, i.e. the probability of observing 2 or less cases.

The same strategy was used to quantify the significance of other descriptions of tradeoffs. We tested whether there is a significantly high probably of obtaining one or more poorer-than-basal score when an improved score (in any metric) is obtained with a parameter set. This analysis was then performed for each pair of metrics, i.e. permutation tests for six conditional probabilities were conducted. In these analyses, empirical right-tail *p*-values were obtained.

CRediT authorship contribution statement

Ziyi Liu: Investigation, Methodology, Visualization, Writing - original draft, Writing - review & editing. **Elena D. Shpak:** Conceptualization, Supervision, Funding acquisition, Writing - original draft, Writing - review & editing. **Tian Hong:** Investigation, Methodology, Visualization, Conceptualization, Supervision, Funding acquisition, Writing - original draft, Writing - review & editing.

Declaration of Competing Interest

The authors declare that they have no known competing financial interests or personal relationships that could have appeared to influence the work reported in this paper.

Acknowledgements

This work was supported by the National Institute of General Medical Sciences of the National Institutes of Health under Award R01GM140462 to TH. This work was supported by the National Science Foundation (grant no. IOS–2016756 to ES). Funding sources had no such involvement in study design; in the collection, analysis and interpretation of data; in the writing of the report; or in the decision to submit the article for publication.

Appendix A. Supplementary data

Supplementary data to this article can be found online at https://doi.org/10.1016/j.csbj.2020.11.017.

References

[1] Scheres B. Stem-cell niches: nursery rhymes across kingdoms. Nat Rev Mol Cell Biol 2007;8(5):345.
[2] Sablowski R. The dynamic plant stem cell niches. Curr Opin Plant Biol 2007;10(6):639–44.
[3] Uchida N, Torii KU. Stem cells within the shoot apical meristem: identity, arrangement and communication. Cell Mol Life Sci 2019;76(6):1067–80.
[4] Kitagawa M, Jackson D. Control of meristem size. Annu Rev Plant Biol 2019;70:269–91.
[5] Han H, Liu X, Zhou Y. Transcriptional circuits in control of shoot stem cell homeostasis. Curr Opin Plant Biol 2020;53:50–6.
[6] Fletcher JC, Brand U, Running MP, Simon R, Meyerowitz EM. Signaling of cell fate decisions by CLAVATA3 in Arabidopsis shoot meristems. Science 1999;283(5409):1911–4.
[7] Laux T, Mayer KF, Berger J, Jurgens G. The WUSCHEL gene is required for shoot and floral meristem integrity in Arabidopsis. Development 1996;122(1):87–96.
[8] Mayer KFX, Schoof H, Haecker A, Lenhard M, Jürgens G, et al. Role of WUSCHEL in regulating stem cell fate in the Arabidopsis shoot meristem. Cell 1998;95(6):805–15.
[9] Schoof H, Lenhard M, Haecker A, Mayer KFX, Jürgens G, et al. The stem cell population of Arabidopsis shoot meristems is maintained by a regulatory loop between the CLAVATA and WUSCHEL genes. Cell 2000;100(6):635–44.
[10] Brand U, Fletcher JC, Hobe M, Meyerowitz EM, Simon R. Dependence of stem cell fate in Arabidopsis on a feedback loop regulated by CLV3 activity. Science 2000;289(5479):617–9.
[11] Yadav RK, Perales M, Gruel J, Girke T, Jönsson H, et al. WUSCHEL protein movement mediates stem cell homeostasis in the Arabidopsis shoot apex. Genes Dev 2011;25(19):2025–30.
[12] Somssich M, Je BI, Simon R, Jackson D. CLAVATA-WUSCHEL signaling in the shoot meristem. Development 2016;143(18):3238–48.
[13] Zhou Y, Yan A, Han H, Li T, Geng Y, et al. HAIRY MERISTEM with WUSCHEL confines CLAVATA3 expression to the outer apical meristem layers. Science 2018;361(6401):502–6.
[14] Shimotohno A, Scheres B. Topology of regulatory networks that guide plant meristem activity: similarities and differences. Curr Opin Plant Biol 2019;51:74–80.
[15] Perales M, Rodriguez K, Snipes S, Yadav RK, Diaz-Mendoza M, et al. Threshold-dependent transcriptional discrimination underlies stem cell homeostasis. Proc Natl Acad Sci U S A 2016;113(41):E6298–306.
[16] Jönsson H, Heisler M, Reddy GV, Agrawal V, Gor V, et al. Modeling the organization of the WUSCHEL expression domain in the shoot apical meristem. Bioinformatics 2005;21(suppl_1):i232–40.
[17] Nikolaev SV, Penenko AV, Lavreha VV, Mjolsness ED, Kolchanov NA. A model study of the role of proteins CLV1, CLV2, CLV3, and WUS in regulation of the structure of the shoot apical meristem. Russian J Develop Biol 2007;38(6):383–8.
[18] Hohm T, Zitzler E, Simon R. A dynamic model for stem cell homeostasis and patterning in Arabidopsis meristems. PLoS ONE 2010;5:2.
[19] Fujita H, Toyokura K, Okada K, Kawaguchi M. Reaction-diffusion pattern in shoot apical meristem of plants. PLoS ONE 2011;6(3):e18243.
[20] Adibi M, Yoshida S, Weijers D, Fleck C. Centering the organizing center in the Arabidopsis thaliana shoot apical meristem by a combination of cytokinin signaling and self-organization. PLoS ONE 2016;11(2):e0147830.
[21] Gruel J, Landrein B, Tarr P, Schuster C, Refahi Y, et al. An epidermis-driven mechanism positions and scales stem cell niches in plants. Sci Adv 2016;2(1):e1500989.
[22] Gruel J, Deichmann J, Landrein B, Hitchcock T, Jönsson H. The interaction of transcription factors controls the spatial layout of plant aerial stem cell niches. npj Syst Biol Appl 2018;4(1):36.
[23] Chickarmane VS, Gordon SP, Tarr PT, Heisler MG, Meyerowitz EM. Cytokinin signaling as a positional cue for patterning the apical–basal axis of the growing Arabidopsis shoot meristem. Proc Natl Acad Sci USA 2012;109(10):4002–7.
[24] Banwarth-Kuhn M, Nematbakhsh A, Rodriguez KW, Snipes S, Rasmussen CG, et al. Cell-based model of the generation and maintenance of the shape and structure of the multilayered shoot apical meristem of Arabidopsis thaliana. Bull Math Biol 2019;81(8):3245–81.
[25] Klawe FZ, Stiehl T, Bastian P, Gaillochet C, Lohmann JU, et al. Mathematical modeling of plant cell fate transitions controlled by hormonal signals. PLoS Comput Biol 2020;16(7):e1007523.
[26] Yadav RK, Tavakkoli M, Reddy GV. WUSCHEL mediates stem cell homeostasis by regulating stem cell number and patterns of cell division and differentiation of stem cell progenitors. Development 2010;137(21):3581–9.
[27] Yadav RK, Perales M, Gruel J, Ohno C, Heisler M, et al. Plant stem cell maintenance involves direct transcriptional repression of differentiation program. Mol Syst Biol 2013;9(1):654.
[28] Kosentka PZ, Overholt A, Maradiaga R, Mitoubsi O, Shpak ED. EPFL signals in the boundary region of the SAM restrict its size and promote leaf initiation. Plant Physiol 2019;179(1):265–79.
[29] Zhang L, DeGennaro D, Lin G, Chai J, Shpak ED (2020) ERECTA family signaling constrains CLAVATA3 and WUSCHEL to the center of the shoot apical meristem. bioRxiv 10.1101/2020.02.24.962787: 2020.2002.2024.962787.
[30] Kimura Y, Tasaka M, Torii KU, Uchida N. ERECTA-family genes coordinate stem cell functions between the epidermal and internal layers of the shoot apical meristem. Development 2018;145. 1:dev156380.
[31] Brand U, Grünewald M, Hobe M, Simon R. Regulation of CLV3 expression by two homeobox genes in Arabidopsis. Plant Physiol 2002;129(2):565–75.
[32] Uchida N, Shimada M, Tasaka M. ERECTA-family receptor kinases regulate stem cell homeostasis via buffering its cytokinin responsiveness in the shoot apical meristem. Plant Cell Physiol 2013;54(3):343–51.
[33] Schulze S, Schäfer BN, Parizotto EA, Voinnet O, Theres K. LOST MERISTEMS genes regulate cell differentiation of central zone descendants in Arabidopsis shoot meristems. Plant J 2010;64(4):668–78.
[34] Müller R, Borghi L, Kwiatkowska D, Laufs P, Simon R. Dynamic and compensatory responses of Arabidopsis shoot and floral meristems to CLV3 signaling. Plant Cell 2006;18(5):1188–98.
[35] Cotterell J, Sharpe J. An atlas of gene regulatory networks reveals multiple three-gene mechanisms for interpreting morphogen gradients. Mol Syst Biol 2010;6:1.
[36] Zagorski M, Tabata Y, Brandenberg N, Lutolf MP, Tkačik G, et al. Decoding of position in the developing neural tube from antiparallel morphogen gradients. Science 2017;356(6345):1379–83.
[37] Clark SE, Running MP, Meyerowitz EM. CLAVATA3 is a specific regulator of shoot and floral meristem development affecting the same processes as CLAVATA1. Development 1995;121(7):2057–67.
[38] Chen M-K, Wilson RL, Palme K, Ditengou FA, Shpak ED. ERECTA family genes regulate auxin transport in the shoot apical meristem and forming leaf primordia. Plant Physiol 2013;162(4):1978–91.
[39] Wang J, Tian C, Zhang C, Shi B, Cao X, et al. Cytokinin signaling activates WUSCHEL expression during axillary meristem initiation. Plant Cell 2017;29(6):1373–87.
[40] Kwiatkowska D. Flowering and apical meristem growth dynamics. J Exp Bot 2008;59(2):187–201.

[41] Williams L, Grigg SP, Xie M, Christensen S, Fletcher JC. Regulation of Arabidopsis shoot apical meristem and lateral organ formation by microRNA miR166g and its AtHD-ZIP target genes. Development 2005;132(16):3657–68.
[42] Rodriguez-Leal D, Xu C, Kwon C-T, Soyars C, Demesa-Arevalo E, et al. Evolution of buffering in a genetic circuit controlling plant stem cell proliferation. Nat Genet 2019;51(5):786–92.
[43] Chung Y, Zhu Y, Wu M-F, Simonini S, Kuhn A, et al. Auxin response factors promote organogenesis by chromatin-mediated repression of the pluripotency gene SHOOTMERISTEMLESS. Nat Commun 2019;10(1):1–11.
[44] Long JA, Moan EI, Medford JI, Barton MK. A member of the KNOTTED class of homeodomain proteins encoded by the STM gene of Arabidopsis. Nature 1996;379(6560):66–9.
[45] Fouracre JP, Poethig RS. Role for the shoot apical meristem in the specification of juvenile leaf identity in Arabidopsis. Proc Natl Acad Sci U S A 2019;116 (20):10168–77.
[46] Han H, Yan A, Li L, Zhu Y, Feng B, et al. A signal cascade originated from epidermis defines apical-basal patterning of Arabidopsis shoot apical meristems. Nat Commun 2020;11(1):1–17.
[47] Knauer S, Holt AL, Rubio-Somoza I, Tucker EJ, Hinze A, et al. A protodermal miR394 signal defines a region of stem cell competence in the Arabidopsis shoot meristem. Dev Cell 2013;24(2):125–32.
[48] Zhao Z, Andersen SU, Ljung K, Dolezal K, Miotk A, et al. Hormonal control of the shoot stem-cell niche. Nature 2010;465(7301):1089–92.
[49] Zhou Y, Liu X, Engstrom EM, Nimchuk ZL, Pruneda-Paz JL, et al. Control of plant stem cell function by conserved interacting transcriptional regulators. Nature 2015;517(7534):377.
[50] Dahmann C, Oates AC, Brand M. Boundary formation and maintenance in tissue development. Nat Rev Genet 2011;12(1):43.
[51] Novak B, Tyson JJ, Gyorffy B, Csikasz-Nagy A. Irreversible cell-cycle transitions are due to systems-level feedback. Nat Cell Biol 2007;9(7):724–8.
[52] Hong T, Oguz C, Tyson JJ. A mathematical framework for understanding four-dimensional heterogeneous differentiation of CD4+ T Cells. Bull Math Biol 2015. https://doi.org/10.1007/s11538-015-0076-6; 1–19.
[53] Hong T, Fung ES, Zhang L, Huynh G, Monuki ES, et al. Semi-adaptive response and noise attenuation in bone morphogenetic protein signalling. J R Soc Interface 2015;12(107):20150258.
[54] Suderman R, Bachman JA, Smith A, Sorger PK, Deeds EJ. Fundamental trade-offs between information flow in single cells and cellular populations. Proc Natl Acad Sci U S A 2017;114(22):5755–60.
[55] Daum G, Medzihradszky A, Suzaki T, Lohmann JU. A mechanistic framework for noncell autonomous stem cell induction in Arabidopsis. Proc Natl Acad Sci U S A 2014;111(40):14619–24.
[56] Lenhard M, Laux T. Stem cell homeostasis in the Arabidopsis shoot meristem is regulated by intercellular movement of CLAVATA3 and its sequestration by CLAVATA1. Development 2003;130(14):3163–73.
[57] Gordon SP, Chickarmane VS, Ohno C, Meyerowitz EM. Multiple feedback loops through cytokinin signaling control stem cell number within the Arabidopsis shoot meristem. Proc Natl Acad Sci U S A 2009;106(38):16529–34.
[58] To JPC, Haberer G, Ferreira FJ, Deruere J, Mason MG, et al. Type-A Arabidopsis response regulators are partially redundant negative regulators of cytokinin signaling. Plant Cell 2004;16(3):658–71.
[59] Leibfried A, To JPC, Busch W, Stehling S, Kehle A, et al. WUSCHEL controls meristem function by direct regulation of cytokinin-inducible response regulators. Nature 2005;438(7071):1172.
[60] Delile J, Herrmann M, Peyriéras N, Doursat R. A cell-based computational model of early embryogenesis coupling mechanical behaviour and gene regulation. Nat Commun 2017;8(1):1–10.
[61] Ye Y, Kang X, Bailey J, Li C, Hong T. An enriched network motif family regulates multistep cell fate transitions with restricted reversibility. PLoS Comput Biol 2019;15(3):e1006855.
[62] Choi K, Medley JK, König M, Stocking K, Smith L, et al. Tellurium: an extensible python-based modeling environment for systems and synthetic biology. Biosystems 2018;171:74–9.
[63] Reddy GV, Meyerowitz EM. Stem-cell homeostasis and growth dynamics can be uncoupled in the Arabidopsis shoot apex. Science 2005;310(5748):663–7.